Mol Cancer Ther. Author manuscript; available in PMC 2010 November 01.

Published in final edited form as:
Mol Cancer Ther. 2010 May ; 9(5): 1219–1233. doi:10.1158/1535-7163.MCT-09-0683.

Mechanistic evaluation of the novel HSP90 inhibitor NVP-AUY922 in adult and pediatric glioblastoma

Nathalie Gaspar[1,2,3], **Swee Y Sharp**[1], **Suzanne A Eccles**[4], **Sharon Gowan**[4], **Sergey Popov**[3], **Chris Jones**[3], **Andrew Pearson**[3], **Gilles Vassal**[2], and **Paul Workman**[1]

[1]Signal Transduction and Molecular Pharmacology Team, Cancer Research UK Centre for Cancer Therapeutics, The Institute of Cancer Research, Sutton, Surrey, UK

[2]UPRES EA 3535, Paris XI University, IFR54, Pharmacology and New Treatments of Cancer and Translational Research Department, Institut de Cancérologie Gustave Roussy, Villejuif, France

[3]Paediatric Drug Development, The Institute of Cancer Research, Sutton, Surrey, SM2 5NG, UK

[4]Tumour Biology and Metastasis, Cancer Research UK Centre for Cancer Therapeutics, The Institute of Cancer Research, Sutton, Surrey, SM2 5NG UK

Abstract

The dismal prognosis of glioblastoma (GB) indicates the urgent need for new therapies for these tumors. Heat shock protein 90 (HSP90) inhibitors induce proteasome-mediated degradation of many oncogenic client proteins involved in all of the hallmark characteristics of cancer. Here, we explored the mechanistic potential of the potent synthetic diarylisoxazole amide resorcinol HSP90 inhibitor, NVP-AUY922, in adult and pediatric GB. *In vitro* antiproliferative potency (nanomolar range) was seen in both adult and pediatric human GB cell lines with different molecular pathologies. A cytostatic effect was observed in all GB lines; more apoptosis was observed at lower concentrations in SF188 pediatric GB line and at 144hrs in the slower growing KNS42 pediatric GB line, as compared to the adult GB lines, U87MG and SF268. *In vitro* combination studies with inhibitors of PI3 kinase/mTOR (PI-103) or MEK (PD-0325901) supported the hypothesis that sustained inhibition of ERK up to 72hrs and at least temporary inhibition of AKT were necessary to induce apoptosis in GB lines. In athymic mice bearing established subcutaneous U87MG glioblastoma xenografts, NVP-AUY922 (50mg/kg i.p x 3 days) caused inhibition of ERK1/2 and AKT phosphorylation and induced apoptosis, while 17-AAG used at MTD was less effective. NVP-AUY922 antitumor activity with objective tumor regression resulted from antiproliferative, pro-apoptotic and anti-angiogenic effects, the latter shown by decreased microvessel density and HIF1α levels. Our results have established mechanistic proof of concept for the potential of novel synthetic HSP90 inhibitors in adult and pediatric GB, alone or in combination with PI3 kinase/mTOR and MEK inhibitors.

Corresponding author: Professor Paul Workman PhD FMedSci FSB, Address: Cancer Research UK Centre for Cancer Therapeutics, The Institute of Cancer Research, Haddow Laboratories, 15 Cotswold Road, Sutton, Surrey SM2 5NG, UK, Phone: +44 (0) 208 722 4301, Fax: +44 (0) 208 722 4324, Paul.Workman@icr.ac.uk.

Conflict of Interest

Professor Paul Workman and his group received research funding on the development of HSP90 inhibitors from Vernalis Ltd and intellectual property from this program was licensed to Vernalis Ltd and Novartis. Nathalie Gaspar, Swee Sharp, Chris Jones, Andrew Pearson, Suzanne Eccles and Paul Workman are employees of The Institute of Cancer Research which has a commercial interest in HSP90 inhibitors under development by Novartis Ltd.

Paul Workman has been a consultant to Novartis and Suzanne Eccles is a consultant for Vernalis.

Europe PMC Funders Author Manuscripts

Keywords

adult glioblastoma; pediatric glioblastoma; HSP90 inhibitors; NVP-AUY922; PD-0325901; PI-103; apoptosis

Introduction

Glioblastomas (GB) are highly invasive primary brain tumors with poor prognosis despite current therapies (surgery, radiotherapy and chemotherapy; ref 1). Targeted therapies, as single agents, have failed to offer long term survival benefit, despite objective initial responses (2). GB heterogeneity and a complex molecular pathology contribute to this lack of success. Thus, GB might be more efficiently eradicated by targeting multiple signaling pathways or different tumor features (proliferation, resistance to apoptosis, angiogenesis, and invasion) simultaneously.

The molecular chaperone heat shock protein 90 (HSP90) regulates the conformation, stability and function of many critical oncogenic client proteins that are essential in maintaining malignant transformation and in increasing the survival, growth and invasive potential of cancer cells (3). HSP90 inhibitors induce proteasome-mediated degradation of these client proteins (3). 17-allylamino-17-demethoxygeldanamycin (17-AAG, tanespimycin), the first-in-class HSP90 inhibitor to enter clinical trials, has shown early signs of clinical activity in adult and pediatric patients with different tumor types (4-6).

Antiproliferative, anti-invasive and pro-apoptotic effects have been observed in *in vitro* adult GB (aGB) cells with ansamycin benzoquinone HSP90 inhibitors such as 17-AAG, and with the structurally unrelated natural product HSP90 inhibitor radicicol (7-11). 17-AAG was also shown to target the glioma stem cells which may initiate tumor recurrences (12). Synergistic interactions have been reported between HSP90 inhibitors and anti-GB therapies, such as radiotherapy (12), SN38 (13), LY294002 (14) and gefitinib (15). However, ansamycin benzoquinones present limitations (eg. suboptimal solubility, cumbersome formulation and extensive metabolism; ref 3). In particular, low activity of the NAD(P)H:quinone oxidoreductase 1 (NQO1/DT-diaphorase) is a factor in intrinsic (16) and acquired resistance to 17-AAG in GB cells (17).

The synthetic pyrazole/isoxazole resorcinol class of HSP90 inhibitors (18-20) offer advantages over 17-AAG, including independence from NQO1 metabolism, PgP insensitivity and favourable aqueous solubility (21, 22). One member of this series, NVP-AUY922, has recently entered phase I clinical trials in adult patients (22). Interestingly, NVP-AUY922 and related agents retain full activity in GB lines rendered resistant to 17-AAG (17). Also, we have been unable to generate resistance to NVP-AUY922 in GB lines by using a continuous drug exposure protocol that did induce 17-AAG resistance (17).

The aim of the present study was to evaluate the mechanistic potential of NVP-AUY922, in both aGB and pediatric human GB (pGB) models. We demonstrate that NVP-AUY922 exhibits a potent anti-GB activity both in *in vitro* cell culture systems and also in *in vivo* sub-cutaneous (s.c.) human GB models driven by different genetic abnormalities, from both adult and pediatric origins. We show that by depleting client proteins involved in the main GB oncogenic pathways, NVP-AUY922 exhibited cytostatic, pro-apoptotic and anti-angiogenic effects, with more extensive apoptosis in the pediatric GB lines studied. We also provide evidence to support the hypothesis that pro-apoptotic effects of NVP-AUY922 depend on the inhibition of both ERK and AKT phosphorylation. Taken together, our results have established mechanistic proof of concept for the potential of novel synthetic HSP90

inhibitors in aGB and pGB, both alone or in combination with PI3 kinase/mTOR and MEK inhibitors.

Materials and Methods

Glioblastoma cell lines

Human GB cell lines from adult (U87MG, SF268) and pediatric (SF188, KNS42) patients were obtained and grown as previously published (17).

Drugs and compounds

HSP90 inhibitors were either purchased or prepared as described (17). The dual PI3 kinase/mTOR inhibitor PI-103 and the MEK inhibitor PD-0325901 were provided by Piramed Ltd and Dundee University, UK, respectively.

Growth inhibition studies

Growth inhibition was determined using the sulforhodamine B assay (SRB; ref 16). Briefly, 10^3 cells were seeded into 96-well microtiter plates and allowed to attach for 36hrs (2×10^3 cells for KNS42). Compounds at a range of concentrations were added in quadruplicate wells for 6 days (at least 3 doubling-times) in a volume of 200μl per well. The IC_{50} was calculated as the drug concentration that inhibits cell proliferation by 50% compared with controls.

Cell viability, cell cycle and apoptosis analysis

Cell count and cell cycle status were determined as described (21), involving the trypan blue exclusion method and DNA content analysis using propidium iodine (PI) staining and flow cytometry, respectively, on the total cells population (attached and detached cells). Sub-G1 population quantification by flow cytometry and PARP and caspase cleavage by immunoblotting were used to confirm apoptosis. The antibody C-2-10 (Clontech, Oxford, UK) recognizing both the 116kDa native PARP and the 85kDa apoptosis-related cleavage product was used, together with anti-caspase antibodies recognising both full length inactive pro-caspases and active cleaved caspases 3, 7, 8 and 9. Antibodies are listed in Supplementary data (Table S1).

Combination studies

Cells were treated with increasing concentrations of drugs either alone or in combination at their equipotent molar ratio concomitantly. Effects on cell number were determined by SRB assay. The results were analyzed using the median effect analysis method (23) and deriving the combination index (CI) which was calculated at ED50 (equipotent combined drug doses that inhibit growth at 50%). Exclusive CI values were used to analyse combinations with agents sharing a similar mechanism of action (HSP90 inhibitors, PI-103 and PD-0325901).

Western blot analysis

Procedures for cell lysate preparation and western blotting were as described (21). Immunodetection was carried out using antibodies listed in Supplementary data (Table S1). Densitometry was performed on the westerns blots by Image Quant Pro software. Results are provided for repeat experiments (n=3). Standard errors for repeat experiments were typically 18-20% of the mean.

Europe PMC Funders Author Manuscripts

Tumor xenograft efficacy studies

Animal procedures were carried out within guidelines set out by The Institute of Cancer Research's Animal Ethics Committee and in compliance with national guidelines (24).

Human U87MG aGB cells (2×10^6) were injected s.c. in the flanks of 8 female NCr athymic mice per group. Animals were treated for 2 weeks with vehicle, NVP-AUY922 or 17-AAG, once tumors reached 8 mm in mean diameter. Tumor volumes and body weights were measured three times a week. Therapeutic activity was determined according to the number of complete responses, partial responses (regression>50%), stable disease, and tumor-free survivors at day 120. Tumor growth delay was calculated as the difference between treated and control groups in the median time to reach a median tumor volume 5 times greater than the initial volume, as described (25). Progression free survival probabilities were calculated using the Kaplan–Meier method.

Biomarker analysis by electrochemiluminescent immunoassay and VEGF analysis by ELISA

Pharmacodynamic biomarker studies were performed on tumor tissues harvested 24 and 48hrs after a 3 day treatment course. Frozen samples were lysed, homogenized and analyzed for protein content, as described (26).

Expression of selected proteins (HSP72, HIF1α, and phosphorylated and total AKT, ERK, and MET), was determined by electrochemiluminescent immunoassay (MesoScale Discovery MSD®), as described (26). VEGF expression was analyzed using a Human Quantikine VEGF ELISA kit (R&D Systems, Abingdon, UK). Briefly, tumor lysates were titrated to determine the optimum amount of protein for the control samples to be within the linear range of the assay. 16ug of protein was loaded per well and the protocol followed as per manufacturer's instructions for serum or plasma samples. Results (pg/ml) were calculated by subtracting readings at 570nm from the readings at 450nm (to correct for optical imperfections in the plate) and determined from the standard curve.

Immunohistochemistry, terminal deoxynucleotidyl transferase-mediated dUTP nick end labelling (TUNEL) and microvessel density analysis

Five μm thick sections of formalin-fixed, paraffin-embedded tumors were prepared. Proliferation index (mouse anti-human Ki67 antibody staining, clone MIB-1, Dako; 1/300 dilution) and apoptosis (TUNEL assay, In situ Cell Death Detection Kit, AP, Roche Diagnostics GmbH, Mannheim, Germany) were determined as described (25). Eight fields per section at x40 objective magnification, randomly selected, were counted.

Mouse blood vessels were stained with rat anti-mouse CD34 antibody (Abcam; dilution 1/50) and microvessel density measured as described (27). Five fields per section at x5 objective magnification, randomly selected, were analyzed with Image-Pro Plus 5.0 software (Media Cybernetics).

Statistical analysis

All values are mean±SD of at least three independent experiments, unless otherwise stated. Statistical significance was calculated by a two-tailed paired t test. Statistical significance between *in vivo* treatment groups and controls in their time to reach five times initial tumor volume was estimated by two-tailed non-parametric Kruskal-Wallis test. $P<0.05$ was considered statistically significant. For Kaplan-Meier curves, differences in progression free survival were tested for statistical significance using a log rank test; $P<0.05$ was considered statistically significant.

Results

NVP-AUY922 induces potent cell growth inhibition in adult and pediatric GB cell lines

The molecular characteristics of the GB cell lines used in this study are described in the Supplementary data (Supplementary Figure S1) and in previous work (17, 28). Our previous studies (22) have shown that NVP-AUY922 exhibits potent activity in a range of cancer cell lines of different origins. NVP-AUY922 exhibited strong antiproliferative effects against both human aGB (U87MG, SF268) and pGB lines (SF188, KNS42) with IC_{50} values by SRB assay in the nanomolar range: 7.8±1.2, 6.1±1.5, 7.6±2.2, 4.8±1.2nM, respectively (Table 1). Two analogs of NVP-AUY922 (VER-50589 and VER-49009) with lower potency against HSP90 (21) demonstrated 8-fold and 82-fold increases in IC_{50} values, respectively.

Sensitivity to HSP90 inhibitors of different chemical classes, as determined by SRB assay, was independent of adult versus pediatric GB cell origins. Cellular potency, as measured by the mean IC_{50} for the four GB lines tested, is higher for NVP-AUY922 than for 17-AAG by a factor of 1.8 in U87MG, 2.0 in SF268, 1.5 in SF188 and 6.2 in KNS42 (Table 1). These differences are generally modest, with the exception of KNS42 where the difference is much greater. When compared to radicicol and the purine BIIB021, NVP-AUY922 is 5 to 9-fold and 10 to 23-fold more potent, respectively.

NQO1 expression can play a role in the sensitivity of cancer cell lines to 17-AAG (16). In a panel of 13 aGB and pGB cell lines, there was no clear relationship between response 17-AAG and NQO1 expression (Table 1, Supplementary Figure S1C); this likely indicates additional factors being involved in sensitivity, as noted for other tumor types (16, 29). However, in contrast to our results with 17-AAG (17), NVP-AUY922 exhibited comparatively high potency in the low NQO1 expressing pGB line KNS42 (Table 1, Supplementary Figure S1C). In addition, in the UW479 pGB cell line that shows undetectable NQO1 expression and is the most resistant to 17-AAG (IC50 = 99.0nM), NVP-AUY922 is 62-fold more potent (IC50 = 1.6nM; Supplementary Figure S1C). The enhanced activity of NVP-AUY922 in GB cell lines resistant to 17-AAG through reduced NQO1 expression was demonstrated in our previous studies (17).

NVP-AUY922 exhibits a potent cytostatic effect due to either G1 or G1/G2 arrest, particularly in pediatric GB cell lines

We previously showed that 17-AAG causes G1 and G2-M cell cycle arrest and induces cytostasis and apoptosis in various cancer cell lines (30). Here, direct measurement of viable cell counts showed that both NVP-AUY922 and 17-AAG (at $5xIC_{50}$ concentrations by SRB assay, Table 1) caused a cytostatic effect up to 48hrs post treatment in all cell lines (Figure1). At 72hrs, in aGB lines (U87MG, SF268) or in the SF188 pGB line treated with 17-AAG, cells regrew in the presence of drug. In the pGB lines, the cytostatic effects were sustained for at least 144hrs in KNS42 cells with both inhibitors, while NVP-AUY922 reduced viable cell numbers in SF188 from 72hrs.

Next, we studied the effects of NVP-AUY922 and 17-AAG on cell cycle distribution and apoptosis markers up to 144hrs (Figure 2). Because of space constraints, results are shown for cell cycle distribution (Figure 2A), and PARP and caspase cleavage (Figure 2C) up to 72hrs, which was most informative period. Data for the sub G1 peaks are shown up to 144hrs (Figure 2B). Both NVP-AUY922 and 17-AAG decreased the S-phase population (<10% of cycling cells) and induced either a G1 or G2 arrest, depending on the cell line and the HSP90 inhibitor (Figure 2A and Supplementary Figure S2A). In all GB lines, both HSP90 inhibitors consistently depleted G1/S-transition proteins together with the HSP90 client protein CDK4 and its partner cyclin D1, whereas a decrease in expression of the

HSP90 client protein CDC2 was observed only in cells arresting in G2 (Figures 2C, S2C; Tables S2A-B; ref 9).

NVP-AUY922 induces apoptotic cell death, particularly in the pediatric GB cell lines

NVP-AUY922-induced apoptosis, as shown by an increased sub-G1 population (Figures 2B, S2B) and cleaved PARP (Figures 2C, S2C;Tables S2A-B), was more predominant in the pGB cell line SF188 compared to the aGB cell lines studied here. At 48 and 72hrs, the apoptotic population in NVP-AUY922-treated SF188 pGB cells represented 37 and 29% of events, respectively (Figure 2B) with correspondingly high levels of cleaved PARP (Figure 2C; Supplementary Table S2A). Apoptosis with NVP-AUY922 was greater than with 17-AAG in the SF188 pGB line (Figures 2B, 2C; Tables S2A). In KNS42 pGB cells, which has the longest doubling time, PARP cleavage was observed from 48hrs, while the sub-G1 population increase occurred later at 144hrs (21% of events) with both HSP90 inhibitors (Supplementary Figure S2B). In contrast to the pGB lines, the apoptotic population never exceeded 12% of events in aGB lines regardless of the HSP90 inhibitor used (Figure 2 and Supplementary Figure S2).

As with 17-AAG, NVP-AUY922 exposure resulted in a time-dependent decrease in uncleaved PARP (upper band; Figure 2C). NVP-AUY922 also caused an increase in cleaved PARP (lower band; Figure 2C) in both U87MG and SF188 cells. It was more difficult to detect cleaved PARP in U87MG cells which are less prone to apoptosis in response to HSP90 inhibitors (Figure 2B), especially with 17-AAG (Figure 2C, left panel, lower band); however, a 2-fold increase in cleaved PARP in response to 17-AAG was detected by densitometry (Supplementary Table S2A). The timing of PARP cleavage paralleled the activation of caspases, as shown by the decrease of the full length pro-caspase levels and/or by an increase in cleaved activated caspase levels (Figures 2C, S2C; Tables S2A-B). Activation of caspases 7 and 8 (extrinsic pathway) was observed with both HSP90 inhibitors. Additional activation of caspase 3 (mitochondrial pathway) occurred in SF188 cells (Figure 2C; Supplementary Table S2A), with a greater intensity in the case of NVP-AUY922 than with 17-AAG (Figures 2C, S2C; Tables S2A-B).

NVP-AUY922 induces the molecular signature of HSP90 inhibition in GB cell lines

Figure 3 shows a set of western blots for the expression of a number of HSP90 client proteins and stress response biomarkers in response to NVP-AUY922 and 17-AAG over a time course up to 72hrs in U87MG, SF268, SF188 and KNS42 cell lines. Effects seen were very reproducible (n=3); Figure 3 is an example of a representative experiment and quantitative data averaged over the 3 repeats are shown in Supplementary Table S2B; SE values were typically 18% of the mean.

Figure 3A shows data for HSP90α, HSP90β, HSP72 and HSP27 as markers of the HSF1-dependent stress response ((3, 31). At 5xIC_{50} antiproliferative concentrations of NVP-AUY922, levels of HSP72 and HSP27 were reproducibly (n=3) increased after 8hrs in all cell lines (Figure 3A, Supplementary Table S2B), except for HSP27 in SF268 cells in which this protein was not expressed (17). Sress protein induction was concentration-dependent and occurred from 1xIC_{50} (lower than the concentration required to deplete HSP90 client proteins; data not shown). Levels of the α and β forms of HSP90, which are the targets of NVP-AUY922 (22), were moderately increased (Figure 3A, Supplementary Table S2B), as shown in other cell types with 17-AAG (32). Overall these results demonstrate a typical HSF1 stress response to NVP-AUY922 treatment in the aGB and pGB lines.

NVP-AUY922 consistently (n=3) depleted the main growth factor receptor tyrosine kinases (RTKs) expressed in GB, namely wild-type EGFR, and the client proteins IGF1R,

PDGFRα, PDGFRβ, C-MET and C-KIT (Figure 3B, Supplementary Table S2B). It can be seen that the extent of, delay in, and duration of RTK depletion were dependent on the RTKs and the individual cell lines concerned. As previously reported (33), ERBB2 was the most sensitive client protein in the hierarchy of responses; it was depleted as early as 8hrs but recovered rapidly in SF268 cells. In this aGB line, a transient early increase in expression of some RTKs (C-MET, PDGFRβ) was also observed at 8hrs followed by depletion of these client proteins, as reported for other clients (34).

Pathways downstream of RTKs were also reproducibly (n=3) and quantifiably (Supplementary Table S2B) inactivated by NVP-AUY922 (Figure 3C). Although not a client protein, NVP-AUY922 decreased the level of phosphorylated ERK1/2 (p-ERK) from 8hrs as a result of depletion of the upstream client proteins such as C-RAF and RTKs. p-ERK inhibition occurred in SF268 cells while no C-RAF depletion and an increase in C-MET and PDGFRβ levels were observed. NVP-AUY922 depleted phosphorylated AKT (p-AKT) more rapidly and to a greater extent than total AKT, as previously published (30). The client protein AKT was depleted to a greater extent and duration in pGB lines when compared to aGB lines (Figure 3C).

In most cases, all client proteins and downstream effectors were depleted or inactivated by 24hrs and recovered by 48hrs post-treatment. Interestingly, no recovery was observed in p-AKT, AKT and p-ERK in the pGB lines after NVP-AUY922 treatment (Figure 3). Recovery of these proteins was observed in aGB lines and in the pGB line SF188 treated with 17-AAG (Figure 3C, Supplementary Table S2C), which appeared to correlate with cell regrowth (Figure 1B). No recovery of p-AKT and p-ERK was observed in KNS42 cells (Figure 3C, Supplementary Table S2C), consistent with the prolonged cytostatic effect and cell death observed after treatment with both HSP90 inhibitors in this cell line (Supplementary Figures S2 A/B).

These results suggest that sustained inhibition of p-AKT and p-ERK might be implicated in the prolonged cytostatic and pro-apoptotic effects of HSP90 inhibition, particularly in the pGB lines.

The pro-apoptotic effect of HSP90 inhibition in GB cell lines is concentration-dependent and associated with sustained inhibition of the ERK pathway

Decreased cell viability and increased apoptosis induced by NVP-AUY922 and 17-AAG, were concentration-dependent in both U87MG aGB (Figure 4) and SF188 pGB cells (Supplementary Figure S3). However, the concentration required to induce apoptosis was lower for NVP-AUY922 than for 17-AAG in both GB lines (10x and 20xIC_{50} for U87MG and 5x and 15xIC_{50} for SF188, respectively), and lower in SF188 as compared with U87MG cells (Figures S3 and 4). Thus, HSP90 inhibitor-induced apoptosis depended on both the drug used and the intrinsic characteristics of the particular GB cells.

Interestingly, in U87MG cells, apoptosis was observed when simultaneous inhibition of p-AKT and p-ERK persisted at 72hrs (Figure 4C, Supplementary Table S2D). When both p-AKT and p-ERK recovered or when p-ERK only (15xIC_{50} of 17-AAG) recovered at 72hrs, no major increase in apoptosis was observed. In SF188 cells, partial recovery in p-AKT levels (15xIC_{50} of 17-AAG) did not impair HSP90 inhibitor-induced apoptosis (Supplementary Figure S3C, Supplementary Table S2E). Thus, these correlative studies showed that apoptosis occurred when both AKT and ERK pathways were inhibited and appeared to require sustained p-ERK inhibition for up to 72hrs.

Combination studies with HSP90, PI3 kinase/mTOR and MEK inhibitors in the U87MG adult GB line

In view of the relatively low level of apoptosis in U87MG cells treated with NVP-AUY922 and to further explore the role of PI3 kinase/mTOR and MAPK pathways in GB apoptosis with this agent, we used the dual PI3 kinase/mTOR inhibitor PI-103 and the MEK inhibitor, PD-0325901. When used singly, both PI-103 and PD-0325901 induced G1 arrest (data not shown; ref 35) without apoptosis (Figure 5A, Supplementary Table S2F). PI-103 decreased p-AKT levels at early time points (data not shown; ref 35) with a recovery at 72hrs while PD-0325901 induced sustained depletion of p-ERK (Figure 5A, Supplementary Table S2F). Cross-talk between signaling pathways led to increased p-ERK and p-AKT by PI-103 and PD-0325901 treatment, respectively (Figure 5A, Supplementary Table S2F).

Having defined the pathway modulation by PI-103 and PD-0325901, we next examined the effect of combination using SRB measurements and median effect analysis (23). Concomitant PI-103/PD-0325901 combination treatment of U87MG cells gave an additive effect (Combination index, CI=1; Figure 5B) and also decreased p-AKT and p-ERK levels compared to those observed with each agent alone, whereas total ERK, total AKT and HSP72 expression remained unchanged. However, no apoptosis was observed (Figure 5A). Thus, the combinatorial inhibition of PI3 kinase/mTOR and MAPK pathways was not sufficient to induce apoptosis in the U87MG GB line, despite additive antiproliferative activity.

Next, when either PI-103 or PD-0325901 was combined with HSP90 inhibitors in U87MG cells, synergism with 17-AAG was observed (CI=0.8 with PI-103 and CI=0.5 with PD-032501; Figure 5B). In combination with NVP-AUY922, additivity (CI=1.0) was seen with PD-0325901 and slight antagonism was observed with PI-103 (CI=1.1; Figure 5B) based on SRB assay data. A higher level of apoptosis occurred when U87MG cells were treated with NVP-AUY922 combined with either PI-103 or PD-0325901, with a sub-G1 population representing 14% and 25% of events, respectively (compared to <2% in controls, $P<0.01$). This was associated with PARP and caspase 3 cleavage (Figure 5A, Supplementary Table S2F). These combinations involving NVP-AUY922 induced similar levels of p-ERK inhibition as with PI-103/PD-0325901 combination; in addition, p-AKT was depleted to a greater extent (Figure 5A, Supplementary Table S2F). When 17-AAG was combined with PD-0325901, apoptosis was induced despite an incomplete p-AKT inhibition at early time points (data not shown) and p-AKT levels remained comparable to the untreated control at 72hrs (Figure 5A, Supplementary Table S2F). These results suggest that sustained PI3 kinase/mTOR pathway inhibition was not necessary for the apoptotic process. Conversely, the recovery of p-ERK seen with with the 17-AAG/PI-103 combination led to a prolonged cytostatic effect without apoptosis (Figure 5A, Supplementary Table S2F), indicating that sustained p-ERK depletion was likely necessary to induce apoptosis.

In the case of SF188 pGB cells, different results were obtained with the combination studies compared to the U87MG aGB cells (Supplementary Figure S4, Supplementary Table S2G). The PI-103/PD-0325901 combination was synergistic and was able to induce apoptosis in SF188 cells despite only an early and temporary decrease in p-AKT (at 24hrs) while p-ERK depletion persisted for up to 72hrs (Supplementary Figure S4C, Supplementary Table S2G). This strong apoptotic effect (as shown by decreased cell viability, sub-G1 population >30%, PARP and caspase 3 cleavage) was also observed when SF188 cells were treated for 72hrs with NVP-AUY922 alone and apoptosis was further increased when NVP-AUY922 was combined with either PI-103 or PD-0325901 (Supplementary Figure S4B). In these combined treatments, p-AKT and p-ERK were reduced to undetectable levels up to 72hrs (Supplementary Figure S4C, Supplementary Table S2G). In contrast to NVP-AUY922,

PI-103 and PD-0325901 combinations with 17-AAG did not induce apoptosis in SF188 cells (Supplementary Figure S4B).

Taken together, the above data demonstrate that increased apoptosis is seen in U87MG and SF188 cells with combinations of NVP-AUY922 plus either the PI3 kinase/mTOR inhibitor PI-103 or the MEK inhibitor PD-0325901; in some cases this increase in apoptosis was observed despite antagonism being seen using median effect analysis, which is based on an SRB readout. The correlative biomarker results suggest that both sustained reduction of p-ERK levels and at least temporary depletion of p-AKT were necessary to induce apoptosis in the two GB cell lines studied. Depending on the GB line, this dual pAKT and pERK depletion was either sufficient (SF188) or required additional factors, as yet unidentified, that are modified by HSP90 inhibition (e.g. in U87MG, depletion of other client proteins) to maximize the apoptotic outcome.

NVP-AUY922 induces tumor regression through antiproliferative, pro-apoptotic and anti-angiogenic effects in adult U87MG GB tumor xenografts

Next, to explore therapeutic effects against GB cells *in vivo*, NVP-AUY922 and 17-AAG were studied in mice bearing established s.c. U87MG aGB xenografts (Figure 6). 17-AAG was administered at the maximum tolerated dose (MTD; 80 mg/kg i.p, 5 d/w for 2 weeks). Tumor growth inhibition with stable disease, regression (<50%) or progression (<25%) was observed in 7/8 animals (Figure 6A). A greater antitumor effect was observed with NVP-AUY922 at a lower dose than the MTD (50mg/kg i.p, 5 d/w for 2 weeks, MTD = 75mg/kg daily dosing), with 2 complete responses, 2 partial responses and 4 stable disease (n=8 animals). At the end of the treatment (day 12), the tumor volume of the NVP-AUY922 treated group had decreased to 69% of the initial volume ($P<0.001$). Tumor regression persisted after cessation of the treatment and 2 animals were free of tumor at 120 days. Thus, NVP-AUY922 and 17-AAG treatment led to significant tumor growth delay of 20 and 15 days, respectively ($P<0.001$, Figure 6A). Analysis of these results using the Kaplan-Meier curves gave very similar values for progression free survival to the tumor growth delay values given above (Supplementary Figure S5).

The therapeutic effects were concordant with the molecular signature of HSP90 inhibition observed after a 3 day treatment course (Figure 6B). Induction of the HSF1 stress response was observed at 24hrs, which then decreased 48hrs post-treatment. The depletion of representative HSP90 client proteins (AKT, HIF1α, MET) and inhibition of their activation (p-AKT, p-MET) and of the downstream RAS/RAF/MAPK pathway (p-ERK) were maintained even at 48hrs post-treatment, particularly with NVP-AUY922.

The antitumor activity of NVP-AUY922 was sustained by antiproliferative, pro-apoptotic, and anti-angiogenic effects. The proliferation index (percentage of Ki67 positive cells) was significantly decreased 24hrs post-NVP-AUY922 treatment compared with controls (36±3% and 41±2%, respectively, $P<0.05$; data not shown). Apoptosis was demonstrated by a significant increase in TUNEL-positive cells and caspase 3 cleavage at 48hrs post-NVP-AUY922 treatment (Figure 6C) and was associated with significant depletion of p-ERK, p-AKT and AKT (Figure 6B). A significant decrease in microvessel density was observed with NVP-AUY922 (Figure 6D), which might be explained, at least in part, by p-AKT, AKT and HIF1α depletion (Figure 6B) and also by VEGFR-2 depletion (27). The levels of VEGF were decreased significantly to 33% of control at 48hrs after treatment with 17-AAG ($P<0.05$) but there was no significant effect with NVP-AUY922 ($P>0.05$). Inhibition and depletion of the client protein MET, which has been implicated in GB cell migration (36), was also observed (Figure 6B).

Discussion

GB is a tumor in which efficient treatment options are limited and new therapies with novel mechanisms of action are urgently required. Natural product HSP90 inhibitors and their derivatives have demonstrated interesting *in vitro* properties against aGB (7-11), but few data have been published using *in vivo* human GB models (12, 22), or in pGB models (17) or with new synthetic HSP90 inhibitors which are devoid of the significant limitations of 17-AAG (22).

The new, potent synthetic diarylisoxazole amide resorcinol HSP90 inhibitor NVP-AUY922 exhibits potent activity in a range of cancer cell lines of different origins (20, 22). Here the effects of NVP-AUY922 and other structurally dissimilar HSP90 inhibitors (6) were evaluated mechanistically in human adult (U87MG and SF268) and pediatric (SF188 and KNS42) GB cell lines. Our results showed that they potently inhibited cell proliferation in all lines tested. Comparing the IC50 measured by SRB assay for NVP-AUY922 versus 17-AAG, NVP-AUY922 is more potent than 17-AAG by a factor of 1.8 in U87MG, 2.0 in SF268, 1.5 in SF188 and 6.2 in KNS42. Thus overall, it can be concluded that NVP-AUY922 showed a modest increase in antiproliferative potency, with a greater differential in the pGB KNS42 cell line. NVP-AUY922 was also more potent than the purine-scaffold HSP90 inhibitor BIIB021 (10 to 23-fold).

Through the combinatorial consequences of HSP90 inhibition, this potent growth inhibitory effect was obtained in GB models exhibiting different genetic abnormalities that are among the most common in primary and secondary aGB, as well also in pGB models (28). Interestingly, cellular fate after NVP-AUY922 treatment differed between the pGB and aGB lines tested. A cytostatic effect was observed in all GB lines; apoptosis was detected at lower concentrations in the SF188 pediatric GB lines and also at 144hrs in the slower growing KNS42 pediatric GB line, as compared to the adult GB lines, U87MG and SF268. Given that only four cell lines were used here, further studies are recommended to explore the universality of the tendency towards greater apoptosis responses in pGB cell lines. The interesting differences between the pGB and aGB lines shown here are consistent with several lines of clinical and molecular evidence suggesting that pGB are different from aGB (28, 37). Consequently, drug testing results obtained from aGB models may not be directly applicable to pGB. Thus, it is crucial to include pGB models in preclinical anti-GB drug development (28).

As observed in other tumor types (22) and in aGB models with ansamycin benzoquinones (12), NVP-AUY922 exhibited *in vitro* antiproliferative (cytostatic) and pro-apoptotic effects, associated with the molecular signature of HSP90 inhibition (induction of HSP72 and HSP27 and depletion of multiple HSP90 client proteins relevant to GB), and were time- and concentration-dependent. NVP-AUY922 depleted the main RTKs involved in GB oncogenesis (EGFR, IGF1R, PDGFRα and β, C-KIT and MET) in an RTK-dependent and cell line-dependent manner, and inhibited and depleted downstream proteins in both the PI3 kinase (e.g. AKT) and RAS/RAF/MAPK (e.g. C-RAF) pathways with efficient inhibition of the downstream MAPK effector, p-ERK. However, correlative studies showed that depletion of RTKs alone did not appear to explain apoptosis in our GB lines. Rather, our results suggest that AKT and ERK inhibition appeared to play a key role in the NVP-AUY922-induced apoptosis seen in pGB lines. We therefore analyzed the relationship between modifications of the AKT/ERK pathways and apoptosis under several conditions of HSP90 inhibition and attempted to dissect the effect of each pathway by using PI3 kinase/mTOR or MEK inhibitors alone and in combination with HSP90 inhibitors in the GB lines. We showed that prolonged inhibition of ERK that was associated with the temporary early inhibition of AKT appeared to be the minimum required to induce GB cell apoptosis. In the

aGB line U87MG, additional factors modified by HSP90 inhibition, yet to identified, must also be necessary. The relationship between AKT/ERK inhibition and NVP-AUY922-induced apoptosis was further confirmed by enhanced antitumor activity in mice bearing established s.c. U87MG xenografts treated with NVP-AUY922, as compared with 17-AAG.

Both AKT and ERK pathways are activated in most aGB patients (2) as well as in a subtype of pGB of particularly poor prognosis that is genetically different from aGB (38). Concomitant activation of both AKT and ERK pathways are necessary to induce GB formation in mice, with oncogenesis being further increased in INK4a/ARF deficient mice which harbor disruption of p53 and RB pathways (39, 40). Our data indicated that either AKT or ERK inhibition alone did not lead to apoptosis, while concomitant AKT and ERK inhibition was sufficient to induce apoptosis in SF188 cells and was necessary but not sufficient in U87MG cells. The kinetics of depletion of these signaling pathways appeared to be important. Note, however, that neither NVP-AUY922-induced changes in the cyclinD/CDK4 (Figure 2C, Supplementary Figure S2C) or p53/p14/HDM2 (data not shown) oncogenic pathways, nor *TP53* mutation correlated with NVP-AUY922-induced apoptosis, as observed in other tumor types (41). Thus, further studies are required to determine which additional factors are important to induce apoptosis in GB lines.

Because GB is the cumulative result of multiple oncogenic changes, targeted therapies are readily bypassed via activation of collateral pathways, as observed when we treated GB cells with either a MEK or a dual PI3 kinase/mTOR inhibitor alone. Also, cross-talk between various RTKs and activation of the downstream PI3 kinase pathway through PTEN loss participate in the lack of responsiveness in GB to anti-EGFR drugs (42-44). Thus, the current trend in GB phase I/II trials is to combine targeted agents to overcome existing or induced combinatorial drivers of malignancy. The capacity of HSP90 inhibitor such as NVP-AUY922 to inhibit several RTKs and downstream pathways is thus an interesting and attractive feature in GB and indicates considerable therapeutic potential, as confirmed herein. Even greater activity might be anticipated by combining HSP90 with other molecularly targeted agents to ensure maximum blockade of oncogenic signaling pathways. 17-AAG was previously reported to cooperate with anti-EGFR (15) and anti-PI3kinase therapies (14) to induce apoptosis in GB cells. Here, we observed that combining NVP-AUY922 with either an PI3 kinase/mTOR or a MEK inhibitor was more efficient in inducing apoptosis in GB cells compared to treatment targeting the PI3 kinase/mTOR and MEK inhibitors (PI-103/PD-0325901) either alone or in combination with each other in the absence of the HSP90 inhibitors. The combination of NVP-AUY922 with these agents was also superior in terms of apoptosis induction when compared to the combination of 17-AAG with these same agents. Finally, combined treatments with HSP90 and MEK inhibitors had a greater pro-apoptotic effect than the combined treatments with HSP90 and PI3 kinase/mTOR inhibitors. Consistent with this, GB initiation in INK4a/ARF null mice was obtained by additional activation of ERK pathway but not by additional AKT activation alone (39, 40). It should be noted that with some combinations (NVP-AUY922/PI-103 in U87MG cells, and NVP-AUY922/PI-103 and NVP-AUY922/PD-0325901 in SF188 cells), the increased apoptosis was seen despite antagonism being demonstrated by median effect analysis. Such an outcome is possible because the median effect analysis is based on an SRB readout which is sensitive to both cell cycle arrest and apoptotic effects. Further studies are required to determine the consequences of the antiproliferative and apoptotic effects of the combinations with respect to tumor response *in vivo*.

In our *in vivo* studies, NVP-AUY922 antitumor activity was demonstrated against s.c. U87MG GB xenografts. Tumor growth delay and progression free survival was associated with antiproliferative and pro-apoptotic effects and with clear HSP90 biomarker modulation, including ERK/AKT inhibition, in the GB xenografts, as we also observed *in vitro*. The

robust *in vivo* molecular responses also correlated with other therapeutic properties of NVP-AUY922, in particular its anti-angiogenic effect. Progression of GB requires activation of angiogenesis which depends on up-regulation of VEGF through AKT at early stages (45) and involving the hypoxia/HIF1α pathway at the latest stages (46), both being present in advanced GB tumors in patients. NVP-AUY922 was shown to inhibit *in vitro* endothelial cell functions associated with angiogenesis and to deplete VEGFR2 and VEGFR3 in human tumor xenografts (22). We observed that NVP-AUY922 depleted both p-AKT and HIF1α and decreased microvessel density, attesting to its anti-angiogenic properties in this model. There may be a contribution to the anti-angiogenic effect of 17-AAG via VEGF depletion but this was not detected with NVP-AUY922. Decreased HIF1α levels under NVP-AUY922 treatment might be the consequence of proteasomal degradation of this HSP90 client protein (10) or reflect inhibition of different regulatory factors including AKT and ERK which stabilize HIF1α protein and enhance HIF1α transcriptional activity (47). In addition, *in vivo* depletion of HSP90 client proteins AKT, HIF1α and MET is consistent with a potential anti-invasive effects of NVP-AYU922. Anti-invasive effects of HSP90 inhibition were reported *in vitro* with the natural product HSP90 inhibitors (radicicol and geldanamycin) and 17-AAG (10, 48) and with NVP-AUY922 in other tumor types (22). This might be important in GB, as migrating cells are more resistant to cell death and lead to GB recurrences and mortality (49).

Interestingly, the same level of *in vivo* efficacy seen with a dose of NVP-AUY922 below the MTD was not achieved at the MTD of 17-AAG. This latter benzoquinone ansamycin HSP90 inhibitor is metabolized by NQO1, a known determinant of acquired resistance to this drug in GB cells (17). We also previously observed NQO1 down-regulation after 10 days treatment with 17-AAG in this *in vivo* aGB model (17), which might contribute to decreased efficiency compared with NVP-AUY922.

In conclusion, GB are tumors in which acceptable treatment options are limited and our results suggest that HSP90 inhibitors may have therapeutic potential in both adult and pediatric patients. Our studies with NVP-AUY922 described herein provide a mechanistic rationale and proof of principal that new synthetic HSP90 inhibitors might represent promising candidates as anti-GB agents. Although the mechanism of action of NVP-AUY922 is generally very similar to that of 17-AAG, this new agent may have potential advantages with respect to increased pro-apoptotic effects seen here in some settings and independence from NQO1 metabolism (17), together with improved formulation and potential for reduced hepatotoxicity due to the absence of the quinone moiety. At this stage our antitumor efficacy studies have been restricted to human GB xenografts grown in the subcutaneous site. Having established proof of concept, it is now clearly important to further evaluate the therapeutic activity of HSP90 inhibitors against GB tumors grown in the intracranial location. This requires HSP90 inhibitors that have appropriate blood-brain barrier penetration. Importantly, a very recent paper has described the promising therapeutic effects of a blood-brain barrier permeable synthetic HSP90 inhibitor against intracerebrally implanted U87MG GB xenografts (50). Thus, such HSP90 inhibitors may represent interesting potential new agents for evaluation against GB in the clinic, alone or in association with other targeted therapies.

Supplementary Material

Refer to Web version on PubMed Central for supplementary material.

Acknowledgments

We thank Gary Box, Melanie Valenti and Alexis de-Haven Brandon (Cancer Therapeutics, The Institute of Cancer Research) for assistance with the human tumor xenograft studies, and for cell and tissue preparations. We also thank Kay Savage (The Breakthrough Breast Cancer Research Centre, The Institute of Cancer Research) and Virginie Marty (Translational Research, Institut de Cancérologie Gustave Roussy) for immunohistochemistry.

Funding

La Fondation de France (n° 2005005855 to N.Gaspar).

Cancer Research UK grants CA309/A8274 to P.Workman; C1178/A4098 to A.Pearson.

We acknowledge NHS funding to the NIHR Biomedical Research Centre.

Paul Workman is a Cancer Research UK Life Fellow.

References

1. Stupp R, Hegi ME, Mason WP, et al. Effects of radiotherapy with concomitant and adjuvant temozolomide versus radiotherapy alone on survival in glioblastoma in a randomised phase III study: 5-year analysis of the EORTC-NCIC trial. Lancet Oncol. 2009
2. Omuro AM, Faivre S, Raymond E. Lessons learned in the development of targeted therapy for malignant gliomas. Mol Cancer Ther. 2007; 6:1909–19. [PubMed: 17620423]
3. Workman P, Burrows F, Neckers L, Rosen N. Drugging the cancer chaperone HSP90: Combinatorial therapeutic exploitation of oncogene addiction and tumor stress. Ann N Y Acad Sci. 2007; 1113:202–16. [PubMed: 17513464]
4. Banerji U, O'Donnell A, Scurr M, et al. Phase I pharmacokinetic and pharmacodynamic study of 17-allylamino, 17-demethoxygeldanamycin in patients with advanced malignancies. J Clin Oncol. 2005; 23:4152–61. [PubMed: 15961763]
5. Weigel BJ, Blaney SM, Reid JM, et al. A phase I study of 17-allylaminogeldanamycin in relapsed/refractory pediatric patients with solid tumors: a Children's Oncology Group study. Clin Cancer Res. 2007; 13:1789–93. [PubMed: 17363534]
6. Taldone T, Gozman A, Maharaj R, Chiosis G. Targeting Hsp90: small-molecule inhibitors and their clinical development. Curr Opin Pharmacol. 2008; 8:370–4. [PubMed: 18644253]
7. Yang J, Yang JM, Iannone M, Shih WJ, Lin Y, Hait WN. Disruption of the EF-2 kinase/Hsp90 protein complex: a possible mechanism to inhibit glioblastoma by geldanamycin. Cancer Res. 2001; 61:4010–6. [PubMed: 11358819]
8. Nomura M, Nomura N, Yamashita J. Geldanamycin-induced degradation of Chk1 is mediated by proteasome. Biochem Biophys Res Commun. 2005; 335:900–5. [PubMed: 16099423]
9. Nomura N, Nomura M, Newcomb EW, Zagzag D. Geldanamycin induces G2 arrest in U87MG glioblastoma cells through downregulation of Cdc2 and cyclin B1. Biochem Pharmacol. 2007; 73:1528–36. [PubMed: 17324379]
10. Zagzag D, Nomura M, Friedlander DR, et al. Geldanamycin inhibits migration of glioma cells in vitro: a potential role for hypoxia-inducible factor (HIF-1alpha) in glioma cell invasion. J Cell Physiol. 2003; 196:394–402. [PubMed: 12811834]
11. Nomura M, Nomura N, Newcomb EW, Lukyanov Y, Tamasdan C, Zagzag D. Geldanamycin induces mitotic catastrophe and subsequent apoptosis in human glioma cells. J Cell Physiol. 2004; 201:374–84. [PubMed: 15389545]
12. Sauvageot CM, Weatherbee JL, Kesari S, et al. Efficacy of the HSP90 inhibitor 17-AAG in human glioma cell lines and tumorigenic glioma stem cells. Neuro Oncol. 2008
13. Flatten K, Dai NT, Vroman BT, et al. The role of checkpoint kinase 1 in sensitivity to topoisomerase I poisons. J Biol Chem. 2005; 280:14349–55. [PubMed: 15699047]
14. Premkumar DR, Arnold B, Jane EP, Pollack IF. Synergistic interaction between 17-AAG and phosphatidylinositol 3-kinase inhibition in human malignant glioma cells. Mol Carcinog. 2006; 45:47–59. [PubMed: 16267832]

15. Premkumar DR, Arnold B, Pollack IF. Cooperative inhibitory effect of ZD1839 (Iressa) in combination with 17-AAG on glioma cell growth. Mol Carcinog. 2006; 45:288–301. [PubMed: 16550610]
16. Kelland LR, Sharp SY, Rogers PM, Myers TG, Workman P. DT-Diaphorase expression and tumor cell sensitivity to 17-allylamino, 17-demethoxygeldanamycin, an inhibitor of heat shock protein 90. J Natl Cancer Inst. 1999; 91:1940–9. [PubMed: 10564678]
17. Gaspar N, Sharp SY, Pacey S, et al. Acquired Resistance to 17-Allylamino-17-Demethoxygeldanamycin (17-AAG, Tanespimycin) in Glioblastoma Cells. Cancer Res. 2009; 69:1966–75. [PubMed: 19244114]
18. Cheung KM, Matthews TP, James K, et al. The identification, synthesis, protein crystal structure and in vitro biochemical evaluation of a new 3,4-diarylpyrazole class of Hsp90 inhibitors. Bioorg Med Chem Lett. 2005; 15:3338–43. [PubMed: 15955698]
19. Dymock BW, Barril X, Brough PA, et al. Novel, potent small-molecule inhibitors of the molecular chaperone Hsp90 discovered through structure-based design. J Med Chem. 2005; 48:4212–5. [PubMed: 15974572]
20. Brough PA, Aherne W, Barril X, et al. 4,5-diarylisoxazole Hsp90 chaperone inhibitors: potential therapeutic agents for the treatment of cancer. J Med Chem. 2008; 51:196–218. [PubMed: 18020435]
21. Sharp SY, Prodromou C, Boxall K, et al. Inhibition of the heat shock protein 90 molecular chaperone in vitro and in vivo by novel, synthetic, potent resorcinylic pyrazole/isoxazole amide analogues. Mol Cancer Ther. 2007; 6:1198–211. [PubMed: 17431102]
22. Eccles SA, Massey A, Raynaud FI, et al. NVP-AUY922: a novel heat shock protein 90 inhibitor active against xenograft tumor growth, angiogenesis, and metastasis. Cancer Res. 2008; 68:2850–60. [PubMed: 18413753]
23. Chou TC. Theoretical basis, experimental design, and computerized simulation of synergism and antagonism in drug combination studies. Pharmacol Rev. 2006; 58:621–81. [PubMed: 16968952]
24. Workman P, Twentyman P, Balkwill F, et al. United Kingdom Co-ordinating Committee on Cancer Research (UKCCCR) Guidelines for the Welfare of Animals in Experimental Neoplasia (Second Edition). Br J Cancer. 1998; 77:1–10.
25. Geoerger B, Gaspar N, Opolon P, et al. EGFR tyrosine kinase inhibition radiosensitizes and induces apoptosis in malignant glioma and childhood ependymoma xenografts. Int J Cancer. 2008; 123:209–16. [PubMed: 18386816]
26. Gowan SM, Hardcastle A, Hallsworth AE, et al. Application of meso scale technology for the measurement of phosphoproteins in human tumor xenografts. Assay Drug Dev Technol. 2007; 5:391–401. [PubMed: 17638539]
27. Sanderson S, Valenti M, Gowan S, et al. Benzoquinone ansamycin heat shock protein 90 inhibitors modulate multiple functions required for tumor angiogenesis. Mol Cancer Ther. 2006; 5:522–32. [PubMed: 16546966]
28. Bax DA, Little SE, Gaspar N, et al. Molecular and phenotypic characterisation of paediatric glioma cell lines as models for preclinical drug development. PLoS ONE. 2009; 4:e5209. [PubMed: 19365568]
29. Douglas M, Lim AR, Porter JR, et al. The antiproliferative activity of the heat shock protein 90 inhibitor IPI-504 is not dependent on NAD(P)H:quinone oxidoreductase 1 activity in vivo. Mol Cancer Ther. 2009; 8:3369–78. [PubMed: 19952119]
30. Hostein I, Robertson D, DiStefano F, Workman P, Clarke PA. Inhibition of signal transduction by the Hsp90 inhibitor 17-allylamino-17-demethoxygeldanamycin results in cytostasis and apoptosis. Cancer Res. 2001; 61:4003–9. [PubMed: 11358818]
31. Banerji U, de Bono J, Judson I, Kaye S, Workman P. Biomarkers in early clinical trials: the committed and the skeptics. Clin Cancer Res. 2008; 14:2512. author reply 3-4. [PubMed: 18413847]
32. Maloney A, Clarke PA, Naaby-Hansen S, et al. Gene and protein expression profiling of human ovarian cancer cells treated with the heat shock protein 90 inhibitor 17-allylamino-17-demethoxygeldanamycin. Cancer Res. 2007; 67:3239–53. [PubMed: 17409432]

33. Citri A, Kochupurakkal BS, Yarden Y. The achilles heel of ErbB-2/HER2: regulation by the Hsp90 chaperone machine and potential for pharmacological intervention. Cell Cycle. 2004; 3:51–60. [PubMed: 14657666]
34. Koga F, Xu W, Karpova TS, McNally JG, Baron R, Neckers L. Hsp90 inhibition transiently activates Src kinase and promotes Src-dependent Akt and Erk activation. Proc Natl Acad Sci U S A. 2006; 103:11318–22. [PubMed: 16844778]
35. Guillard S, Clarke PA, Te Poele R, et al. Molecular pharmacology of phosphatidylinositol 3-kinase inhibition in human glioma. Cell Cycle. 2009; 8:443–53. [PubMed: 19177002]
36. Birchmeier C, Birchmeier W, Gherardi E, Vande Woude GF. Met, metastasis, motility and more. Nat Rev Mol Cell Biol. 2003; 4:915–25. [PubMed: 14685170]
37. Broniscer A, Gajjar A. Supratentorial high-grade astrocytoma and diffuse brainstem glioma: two challenges for the pediatric oncologist. Oncologist. 2004; 9:197–206. [PubMed: 15047924]
38. Faury D, Nantel A, Dunn SE, et al. Molecular profiling identifies prognostic subgroups of pediatric glioblastoma and shows increased YB-1 expression in tumors. J Clin Oncol. 2007; 25:1196–208. [PubMed: 17401009]
39. Uhrbom L, Dai C, Celestino JC, Rosenblum MK, Fuller GN, Holland EC. Ink4a-Arf loss cooperates with KRas activation in astrocytes and neural progenitors to generate glioblastomas of various morphologies depending on activated Akt. Cancer Res. 2002; 62:5551–8. [PubMed: 12359767]
40. Lyustikman Y, Momota H, Pao W, Holland EC. Constitutive activation of Raf-1 induces glioma formation in mice. Neoplasia. 2008; 10:501–10. [PubMed: 18472967]
41. Stuhmer T, Zollinger A, Siegmund D, et al. Signalling profile and antitumour activity of the novel Hsp90 inhibitor NVP-AUY922 in multiple myeloma. Leukemia. 2008
42. Stommel JM, Kimmelman AC, Ying H, et al. Coactivation of receptor tyrosine kinases affects the response of tumor cells to targeted therapies. Science. 2007; 318:287–90. [PubMed: 17872411]
43. Chakravarti A, Loeffler JS, Dyson NJ. Insulin-like growth factor receptor I mediates resistance to anti-epidermal growth factor receptor therapy in primary human glioblastoma cells through continued activation of phosphoinositide 3-kinase signaling. Cancer Res. 2002; 62:200–7. [PubMed: 11782378]
44. Mellinghoff IK, Wang MY, Vivanco I, et al. Molecular determinants of the response of glioblastomas to EGFR kinase inhibitors. N Engl J Med. 2005; 353:2012–24. [PubMed: 16282176]
45. Pore N, Liu S, Haas-Kogan DA, O'Rourke DM, Maity A. PTEN mutation and epidermal growth factor receptor activation regulate vascular endothelial growth factor (VEGF) mRNA expression in human glioblastoma cells by transactivating the proximal VEGF promoter. Cancer Res. 2003; 63:236–41. [PubMed: 12517803]
46. Hendriksen EM, Span PN, Schuuring J, et al. Angiogenesis, hypoxia and VEGF expression during tumour growth in a human xenograft tumour model. Microvasc Res. 2008
47. Bardos JI, Ashcroft M. Hypoxia-inducible factor-1 and oncogenic signalling. Bioessays. 2004; 26:262–9. [PubMed: 14988927]
48. Xie Q, Gao CF, Shinomiya N, et al. Geldanamycins exquisitely inhibit HGF/SF-mediated tumor cell invasion. Oncogene. 2005; 24:3697–707. [PubMed: 15782129]
49. Lefranc F, Brotchi J, Kiss R. Possible future issues in the treatment of glioblastomas: special emphasis on cell migration and the resistance of migrating glioblastoma cells to apoptosis. J Clin Oncol. 2005; 23:2411–22. [PubMed: 15800333]
50. Bao R, Lai CJ, Qu H, et al. CUDC-305, a novel synthetic HSP90 inhibitor with unique pharmacologic properties for cancer therapy. Clin Cancer Res. 2009; 15:4046–57. [PubMed: 19509149]

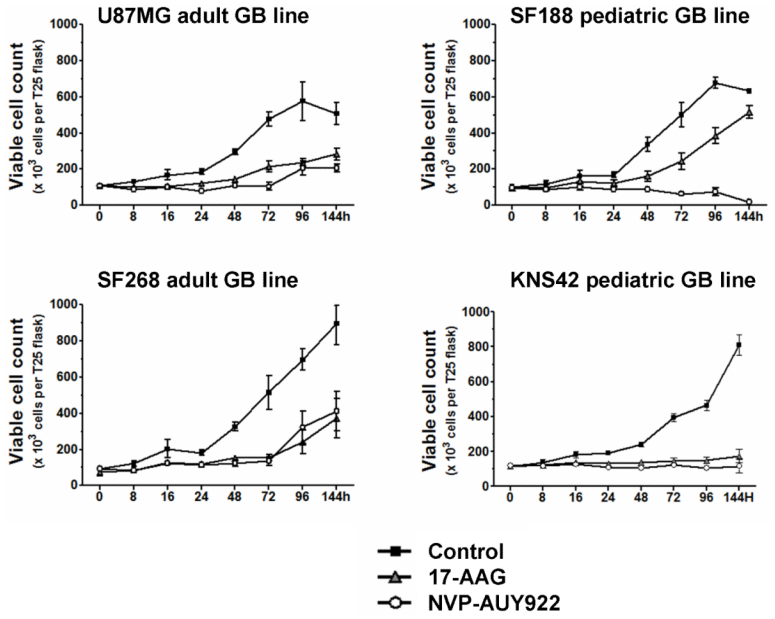

Figure 1. Potent cell growth inhibition induced by NVP-AUY922 in adult and pediatric GB cell lines, as compared to 17-AAG

Effect on absolute viable cell count (trypan blue-excluding cells) in GB lines treated with 5xIC_{50} concentrations (determined by SRB assay) of NVP-AUY922 (○) and 17-AAG (▲), as compared to untreated controls (■). All results are mean±SD of at least 3 independent experiments.

Europe PMC Funders Author Manuscripts

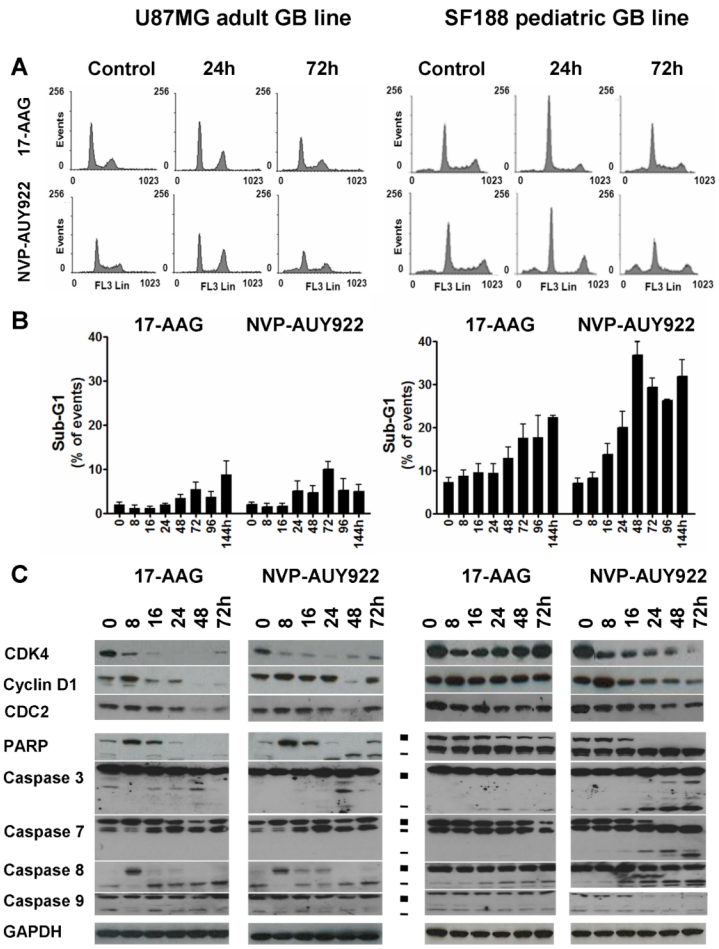

Figure 2. Cell cycle and pro-apoptotic effect of NVP-AUY922 and 17-AAG in adult and pediatric GB cell lines

The adult (U87MG) and the pediatric (SF188) GB lines were treated with 5xIC_{50} concentrations (determined by SRB assay) of either NVP-AUY922 or 17-AAG at time 0 and harvested at indicated time points. **A**- Cell cycle profile at representative time points determine by DNA content analysis using propidium iodine (PI) staining and flow cytometry, **B**- Sub-G1 population as a percentage of total events, as determined by flow cytometry. Values are mean±SD of at least 3 independent experiments. **C**- Immunoblotting analysis of G1/S (CDK4, cyclin D1), G2/M (CDC2) cell cycle transition proteins, PARP and caspase cleavage (■ full length and - cleaved fragments). GAPDH was used as loading control. Results are representative of at least 3 independent experiments. Densitometry data corresponding to the western blots in Figure 2C and repeat experiments which gave similar results are shown in Supplementary Table S2A (n=3; the standard error expressed as a percent of mean was calculated and found to have an overall mean value of 20.3%).

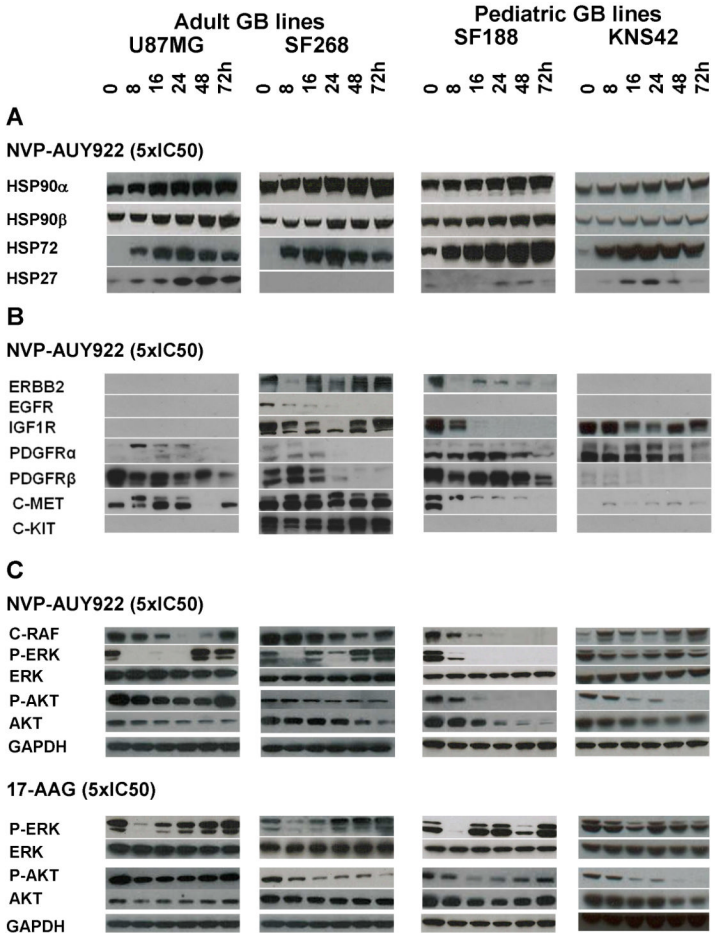

Figure 3. Molecular signature of HSP90 inhibition induced by NVP-AUY922 in adult and pediatric GB cell lines

Western blots of cell lysates from the adult (U87MG, SF268) and the pediatric (SF188, KNS42) GB lines treated with 5xIC_{50} concentrations (determined by SRB assay) of NVP-AUY922 over 72hrs. **A**- Induction of the HSF1-dependent stress response. **B**- Depletion of the main receptor tyrosine kinases (RTKs) involved in GB oncogenesis. **C**- Inhibition of RTK downstream pathways by NVP-AUY922 compared to modifications induced by 5xIC50 concentrations of 17-AAG. GAPDH was used as loading control. Densitometry data corresponding to the western blots in Figure 3 and repeat experiments which gave similar results are shown in Supplementary Table S2B (n=3; the standard error expressed as a percent of mean was calculated and found to have an overall mean value of 17.7%).

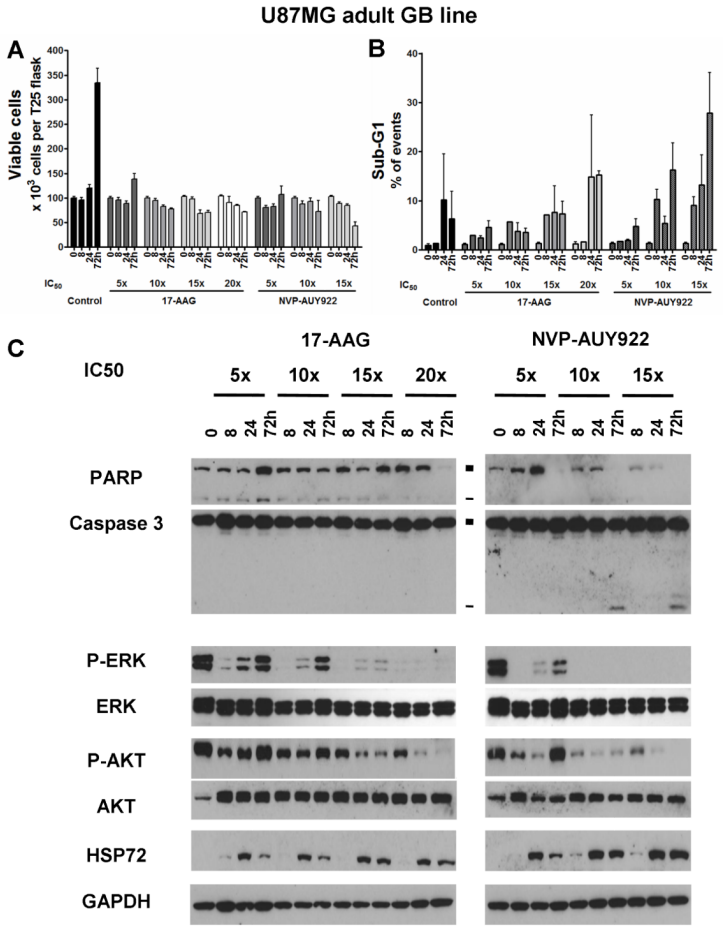

Figure 4. Concentration-dependent pro-apoptotic effect of HSP90 inhibition in the adult GB cell line U87MG

A- Absolute viable cell count using trypan blue-exclusion after treatment with either NVP-AUY922 or 17-AAG at 5, 10, 15 and 20xIC_{50} concentrations, as determined by SRB assay. **B**- Percentage of cells with sub-G1 as analysed by flow cytometry. Results are presented as mean±SD of at least 3 independent experiments. **C**- Immunoblot analysis of caspase dependent apoptosis (PARP and caspase 3 cleavage; ■ full length and - cleaved fragments) and downstream ERK/AKT phosphorylation after treatment with 17-AAG or NVP-AUY922. Densitometry data corresponding to the western blots in Figure 4C and repeat experiments which gave similar results (n=3) are shown in Supplementary Table S2C.

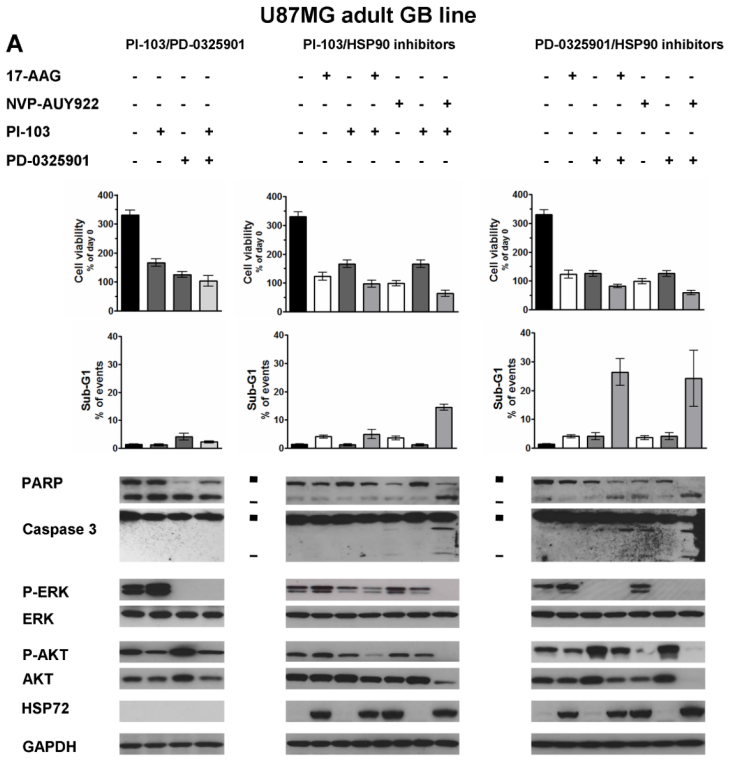

B

	U87MG		
Combination Index (CI)	**PI-103**	**17-AAG**	**NVP-AUY922**
PI-103	-	0.8 ± 0.1	1.1 ± 0.3
PD-0325901	1.0 ± 0.2	0.5 ± 0.2	1.0 ± 0.5

Values are means ± SD from at least 3 independent experiments

Figure 5. Pro-apoptotic effect of combined treatments with HSP90 inhibitors and PI3 kinase/ mTOR inhibitor (PI-103) or the MEK inhibitor (PD-0325901) in the adult GB cell line U87MG

A- Cell viability and analysis of the sub-G1 population by flow cytometry. Immunoblotting (PARP and caspase 3 cleavages; ■ full length and - cleaved fragments) and inhibition of ERK/AKT phosphorylation. GAPDH was used as loading control. Results are representative of at least 3 independent experiments. Densitometry data corresponding to the western blots in Figure 5A and repeat experiments which gave similar results (n=3) are shown in Supplementary Table S2D. **B**- Exclusive combination index (CI) calculated at ED50 (equipotent combined drug concentrations that inhibit growth at 50%) as determined by the median effect analysis method (23). CI<0.9 indicates synergy, CI=1 indicates additivity and CI>1.1 indicates antagonism. All values are mean±SD of n=3 independent experiments. Corresponding results for SF188 cells are provided in Supplementary data (Supplementary Figure S3).

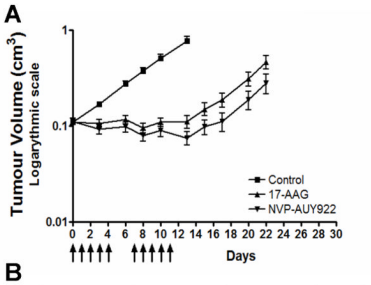

B

T/C (%)	17-AAG		NVP-AUY922	
	24h	48h	24h	48h
HSP72	344	246	360	173
P-ERK	87	89	112	43**
ERK	128	89	132	96
P-AKT	78	70	102	36*
AKT	52*	68	90	55*
HIF1α	144	90	70	64**
P-MET	33*	36	28*	11**
MET	44	45	39*	20**
VEGF	55	33*	198	85

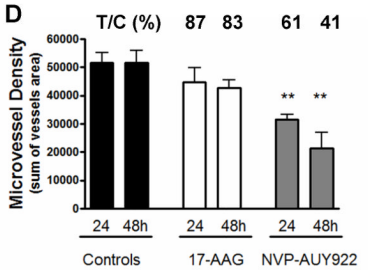

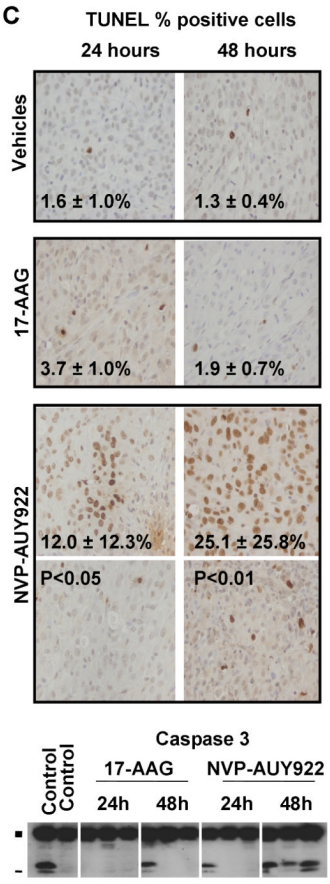

Figure 6. *In vivo* effect of NVP-AUY922 and 17-AAG in the adult U87MG GB subcutaneous tumor xenografts

Control mice received vehicle only (10% DMSO, 5% Tween 20, 85% saline as control for NVP-AUY922, and 43% ethanol, 33% propylene glycol, 24% cremaphor as control for 17-AAG). Treated mice received either 80 mg/kg ip once daily 17-AAG (maximal tolerated dose) or 50 mg/kg once daily NVP-AUY922 (below the maximal tolerated dose). **A**- Antitumor activity of a 2 week treatment (5d/7) by either NVP-AUY922 (▼) or 17-AAG (▲), compared to vehicle controls (■). Arrows (↑) indicate the days of drug administration. **B**- Biomarker modulation using protein quantification by electrochemiluminescent immunoassay (MesoScale Discovery) except for VEGF which was determined by ELISA. Results are given as the percentage of protein level in the treated group as compared to control group at the corresponding time point (% T/C). **C**- Apoptosis was assessed by caspase 3 cleavage (immunoblotting; ■ full length inactive and - cleaved active fragments) and DNA fragmentation analysis (terminal deoxynucleotidyl transferase-mediated dUTP nick end labeling, TUNEL). Representative images are shown at 40x objective magnification for each treatment group, at 24 or 48hrs after a 3 day-treatment course. Two panels are shown for the NVP-AUY922 group as distribution of TUNEL positive cell throughout each sample were unequal. Values shown are mean of percentage of positive cells in 8 fields of view. **D**- Microvessel density analysis by immunohistochemistry staining in mouse endothelial cells by rat anti-CD34 antibody. The histograms shows results expressed as the sum of vessel areas in the fields of view (x5 objective magnitude).

Significant P <0.05 (*) and <0.01 (**). Above the histograms, the values show percent treated over control (% T/C) for the drug treatment.

Table 1

Cell growth inhibition effect of HSP90 inhibitors as measured by sulforhodamine B assay in GB cell lines

IC_{50} values of NVP-AUY922, its less potent analogs VER-50589 and VER-49009, the natural product radicicol, the ansamycin benzoquinones 17-AAG and 17-DMAG, and the synthetic purine scaffold HSP90 inhibitor BIIB021, in 2 adult (U87MG, SF268) and 2 pediatric (SF188, KNS42) GB lines.

	Adult cell lines		Pediatric cell lines	
IC_{50} (nM)	**U87MG**	**SF268**	**SF188**	**KNS42**
NVP-AUY922	7.8 ± 1.2	6.1 ± 1.5	7.6 ± 2.2	4.8 ± 2.1
VER-50589	57.1 ±20.8	28.0 ± 10.8	54.4 ±14.1	57.6 ± 31.2
VER-49009	587.8 ± 99.3	414.2 ± 20.3	328.3 ± 11.9	681.0 ± 150.4
Radicicol	44.9 ± 4.9	32.4 ± 12.0	35.2 ± 5.7	41.3 ± 21.1
17-AAG	13.9 ± 2.0	12.4 ± 0.6	11.2 ± 0.6	29.7 ± 2.3
17-DMAG	3.7 ± 1.3	3.2 ± 1.4	3.3 ± 0.4	3.1 ± 0.2
BIIB021	75.1 ± 47.0	80.5 ± 39.0	142.1 ± 89.7	109.6 ± 29.9

Values are mean ± SD from at least 3 independent experiments